Exploiting broad-area surface emitting lasers to manifest the path-length distributions of finite-potential quantum billiards

Y. T. Yu, P. H. Tuan, K. C. Chang, Y. H. Hsieh, K. F. Huang, and Y. F. Chen*

Department of Electrophysics, National Chiao Tung University, Hsinchu, Taiwan
*yfchen@cc.nctu.edu.tw

Abstract: Broad-area vertical-cavity surface-emitting lasers (VCSELs) with different cavity sizes are experimentally exploited to manifest the influence of the finite confinement strength on the path-length distribution of quantum billiards. The subthreshold emission spectra of VCSELs are measured to obtain the path-length distributions by using the Fourier transform. It is verified that the number of the resonant peaks in the path-length distribution decreases with decreasing the confinement strength. Theoretical analyses for finite-potential quantum billiards are numerically performed to confirm that the mesoscopic phenomena of quantum billiards with finite confinement strength can be analogously revealed by using broad-area VCSELs.

OCIS codes: (250.7260) Vertical cavity surface emitting lasers; (230.7370) Waveguides; (300.6280) Spectroscopy, fluorescence and luminescence.

References and links

1. C. Gmachl, F. Capasso, E. E. Narimanov, J. U. Nöckel, A. D. Stone, J. Faist, D. L. Sivco, and A. Y. Cho, "High-power directional emission from microlasers with chaotic resonators," Science **280**(5369), 1556–1564 (1998).
2. J. A. Hudgings, S. F. Lim, G. S. Li, W. Yuen, K. Y. Lau, and C. J. Chang-Hasnain, "Compact, integrated optical disk readout head using a novel bistable vertical cavity surface emitting laser," IEEE Photonics Technol. Lett. **11**(2), 245–247 (1999).
3. K. Iga, "Surface-emitting laser—Its birth and generation of new optoelectronics field," IEEE J. Sel. Top. Quantum Electron. **6**(6), 1201–1215 (2000).
4. K. J. Vahala, "Optical microcavities," Nature **424**(6950), 839–846 (2003).
5. M. Choi, S. Shinohara, and T. Harayama, "Dependence of far-field characteristics on the number of lasing modes in stadium-shaped InGaAsP microlasers," Opt. Express **16**(22), 17554–17559 (2008).
6. J. Wiersig and M. Hentschel, "Combining directional light output and ultralow loss in deformed microdisks," Phys. Rev. Lett. **100**(3), 033901 (2008).
7. M. Lebental, N. Djellali, C. Arnaud, J. S. Lauret, J. Zyss, R. Dubertrand, C. Schmit, and E. Bogomolny, "Inferring periodic orbits from spectra of simply shaped microlasers," Phys. Rev. A **76**(2), 023830 (2007).
8. W. Fang, H. Cao, and G. S. Solomon, "Control of lasing in fully chaotic open microcavities by tailoring the shape factor," Appl. Phys. Lett. **90**(8), 081108 (2007).
9. D. Dragoman and M. Dragoman, *Quantum-Classical Analogies* (Springer-Verlag, 2004), and references cited therein.
10. K. F. Huang, Y. F. Chen, H. C. Lai, and Y. P. Lan, "Observation of the wave function of a quantum billiard from the transverse patterns of vertical cavity surface emitting lasers," Phys. Rev. Lett. **89**(22), 224102 (2002).
11. T. Gensty, K. Becker, I. Fischer, W. Elsäßer, C. Degen, P. Debernardi, and G. P. Bava, "Wave chaos in real-world vertical-cavity surface-emitting lasers," Phys. Rev. Lett. **94**(23), 233901 (2005).
12. Y. F. Chen, Y. T. Yu, Y. J. Huang, P. Y. Chiang, K. W. Su, and K. F. Huang, "Extracting photon periodic orbits from spontaneous emission spectra in laterally confined vertically emitted cavities," Opt. Lett. **35**(16), 2723–2725 (2010).
13. Y. F. Chen, Y. T. Yu, P. Y. Chiang, P. H. Tuan, Y. J. Huang, H. C. Liang, and K. F. Huang, "Manifestation of quantum-billiard eigenvalue statistics from subthreshold emission of vertical-cavity surface-emitting lasers," Phys. Rev. E Stat. Nonlin. Soft Matter Phys. **83**(1), 016208 (2011).
14. M. Schulz-Ruhtenberg, I. V. Babushkin, N. A. Loiko, T. Ackemann, and K. F. Huang, "Transverse patterns and length-scale selection in vertical-cavity surface-emitting lasers with a large square aperture," Appl. Phys. B **81**(7), 945–953 (2005).

#251204 Received 30 Sep 2015; revised 9 Dec 2015; accepted 9 Dec 2015; published 4 Jan 2016

15. M. Schulz-Ruhtenberg, Y. Tanguy, K. F. Huang, R. Jäger, and T. Ackemann, "Control of the spatial emission structure of broad-area vertical-cavity surface-emitting lasers by feedback," J. Phys. D Appl. Phys. **42**(5), 055101 (2009).
16. I. V. Babushkin, M. Schulz-Ruhtenberg, N. A. Loiko, K. F. Huang, and T. Ackemann, "Coupling of polarization and spatial degrees of freedom of highly divergent emission in broad-area square vertical-cavity surface-emitting lasers," Phys. Rev. Lett. **100**(21), 213901 (2008).
17. D. Wintgen, "Connection between long-range correlations in quantum spectra and classical periodic orbits," Phys. Rev. Lett. **58**(16), 1589–1592 (1987).
18. M. C. Guztwiller, *Chaos in Classical and Quantum Mechanics* (Springer-Verlag, 1990).
19. M. Brack and R. K. Badhuri, *Semiclassical Physics* (Addison-Wesley, 1997).
20. J. D. Jackson, *Classical Electrodynamics* (Wiley, 1975), Chap. 8.
21. E. Bogomolny, R. Dubertrand, and C. Schmit, "Trace formula for dielectric cavities: General properties," Phys. Rev. E Stat. Nonlin. Soft Matter Phys. **78**(5), 056202 (2008).
22. S. Bittner, E. Bogomolny, B. Dietz, M. Miski-Oglu, P. Oria Iriarte, A. Richter, and F. Schäfer, "Experimental test of a trace formula for two-dimensional dielectric resonators," Phys. Rev. E Stat. Nonlin. Soft Matter Phys. **81**(6), 066215 (2010).
23. S. Bittner, E. Bogomolny, B. Dietz, M. Miski-Oglu, and A. Richter, "Application of a trace formula to the spectra of flat three-dimensional dielectric resonators," Phys. Rev. E Stat. Nonlin. Soft Matter Phys. **85**(2), 026203 (2012).
24. F. Lackner, I. Březinová, J. Burgdörfer, and F. Libisch, "Semiclassical wave functions for open quantum billiards," Phys. Rev. E Stat. Nonlin. Soft Matter Phys. **88**(2), 022916 (2013).
25. G. R. Hadley, "Effective index model for vertical-cavity surface-emitting lasers," Opt. Lett. **20**(13), 1483–1485 (1995).
26. E. A. J. Marcatili, "Dielectric rectangular waveguide and directional coupler for integrated optics," Bell Syst. Tech. J. **48**(7), 2071–2102 (1969).

1. Introduction

Optical resonators have been extensively used in numerous applications including lasers, optoelectronic circuits, optical communications, and biological sensors [1–6]. Based on the similarities between the Schrödinger and Helmholtz equations, laser resonators have remarkably exploited to serve as analogous experiments for exploring the mesoscopic physics of quantum systems [6–13]. One of the intriguing analogous experiments is that the lasing transverse modes of broad-area oxide-confined vertical-cavity surface-emitting lasers (VCSELs) can be used to manifest the high-lying eigenmodes of two-dimensional (2D) quantum billiards [10, 14–16]. The lateral confinement of VCSELs is similar to that of the dielectric waveguide, stemming from the difference of the refractive index between the semiconductor medium (n_1) and the surrounding oxide layer (n_2).

In addition to high-order lasing modes, the subthreshold emission spectra of VCSELs are further employed to reveal the path-length distribution of quantum billiards [12, 13]. The path-length distribution is the Fourier transform of the density of state $\rho(k) = \sum_n \delta(k - k_n)$, where k_n are the eigenvalues of quantum billiards. Since the peak positions of the path-length distribution correspond to the lengths of classical periodic orbits (POs), the quantum-classical connection of the system can be directly manifested with the path-length distribution [17–19]. The confinement strength of quantum billiards is usually assumed to be infinite in studying the eigenvalues as well as the path-length distribution. However, the confinement strength is not infinite not only in real quantum systems but also in optical resonators [20–24]. Nevertheless, the influence of the finite confinement strength on the path-length distribution has not been theoretically and experimentally explored as yet.

The effective strength of the confinement can be directly characterized with the number of the allowed eigenmodes. In a one-dimensional (1D) quantum box the number of allowed eigemmodes can be approximately given by $N = a\sqrt{2\mu V_B}\,/\,\pi\hbar$, where a is the box width, V_B is the boundary potential, and μ is the mass of the particle. In other words, the confinement strength can be varied either by the size a or by the potential barrier V_B. Similarly, the number of allowed eigemmodes in 1D dielectric waveguide can be expressed as $N = dk\sqrt{\left(n_1^2 - n_2^2\right)}\,/\,\pi$, where d is the cavity size, k is the wave number, and n_1 and n_2 are the

#251204 Received 30 Sep 2015; revised 9 Dec 2015; accepted 9 Dec 2015; published 4 Jan 2016

refractive indices of the core and cladding regimes, respectively. It is clear that the confinement strength in the dielectric waveguide can be adjusted either by the size *d* or by the amplitude of $n_1^2 - n_2^2$ that plays an analogous role as the potential barrier V_B in the quantum system. Practically, it is more straightforward to control the confinement strength by varying the cavity size *d* instead of varying $n_1^2 - n_2^2$ in using VCSELs to explore the influence of the confinement strength on the path-length distribution. Although the confinement strength would intuitively be a significant parameter in the path-length distribution of VCSELs, the investigation about its role has not been performed in our previous works [12, 13].

In this work we experimentally and theoretically verify that the broad-area VCSELs can be exploited to manifest the influence of the finite confinement strength on the path-length distribution of quantum billiards. We first design several broad-area VCSELs with different cavity sizes to experimentally measure the subthreshold emission spectra. By using the Fourier transform, the path-length distributions are numerically calculated from the measured subthreshold emission spectra. Numerical results reveal that the number of the resonant POs becomes less and less when smaller and smaller cavity size is used. Theoretical analyses for finite-potential quantum billiards are systematically performed to make a thorough comparison with experimental observations. The good agreement between the experimental results and theoretical calculations confirms that the mesoscopic phenomena of finite-potential quantum billiards can be analogously manifested by using broad-area VCSELs.

2. Device design and experiments

We fabricated square-shaped VCSELs with three different cavity sizes, 20 × 20 μm^2, 30 × 30 μm^2, and 40 × 40 μm^2, to measure the subthreshold emission spectra. The VCSEL devices were grown with metal organic chemical vapor deposition. Each laser device consists of a vertical cavity formed by distributed Bragg reflector (DBR) mirrors and a multiple quantum-well active region. The active region was composed of three 70 Å $Al_{0.07}Ga_{0.93}As$ quantum wells alternated with 100 Å $Al_{0.36}Ga_{0.64}As$ barrier layers. The longitudinal wave number is given $k_z = 2\pi/\lambda_o$, where the values of λ_o is designed to be approximately 780 nm. The top and bottom DBR mirrors respectively comprise 23 and 29 double layers. The double layers were formed by an $Al_{0.3}Ga_{0.7}As$ and an $Al_{0.97}Ga_{0.03}As$ layer. The high-Al composition $Al_{0.97}Ga_{0.03}As$ layer at the first p-type DBR mirror was oxidized to define an aperture for current confinement. This oxide aperture forms a planar waveguide and can simultaneously induce an optical confinement. With the parameters of the device structure, the effective index in the medium and the surrounding oxide are obtained to be approximately n_1 = 3.40 and n_2 = 3.37 [25].

The VCSEL devices were driven by a current source with a precision of 0.01 mA. The operating temperature of the VCSELs was controlled by a temperature-controlled system with a stability of 0.1 °C near room temperature. The subthreshold emission spectra of the radiation output were measured by a high-resolution optical spectrum analyzer (Advantest Q8347) with a resolution up to 0.002 nm. With the identity $k_t = \sqrt{(2\pi/\lambda)^2 - k_z^2}$, the measured subthreshold emission spectra $\rho(\lambda)$ can be changed from a function of the emission wavelength λ to a function of the transverse wave number k_t.

First of all, we present a brief synopsis for the characteristics of spontaneous emission spectra emitted from oxide-confined VCSELs. The spontaneous emission spectra of VCSELs

#251204 Received 30 Sep 2015; revised 9 Dec 2015; accepted 9 Dec 2015; published 4 Jan 2016

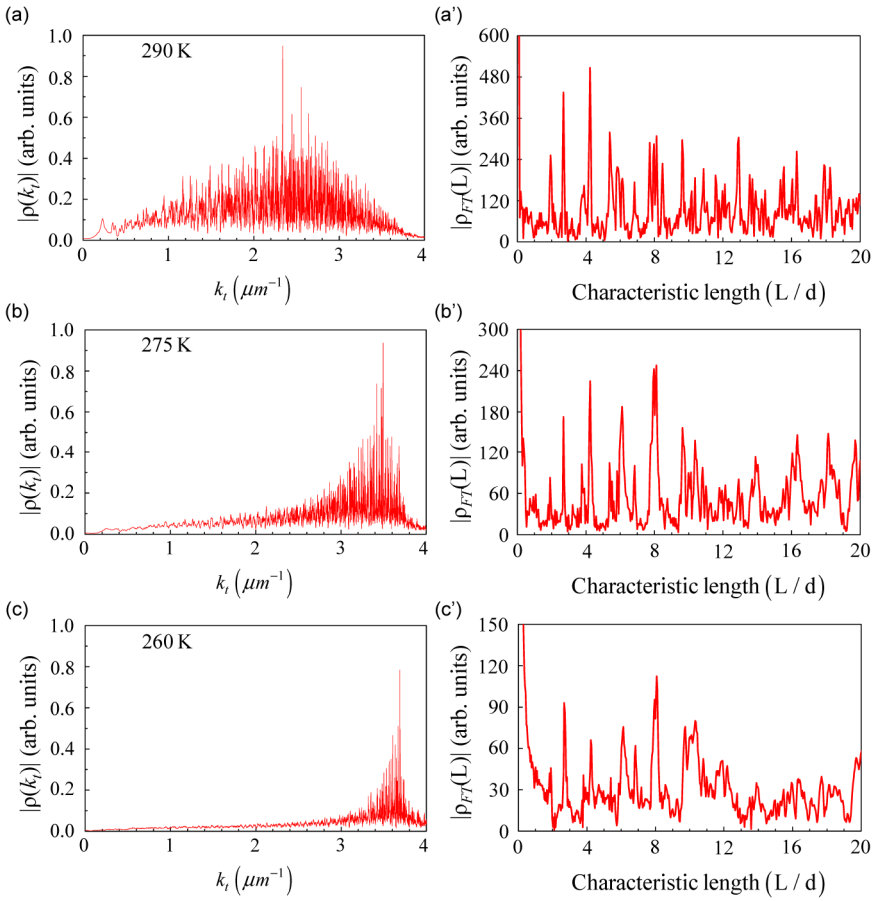

Fig. 1. The subthreshold emission spectra for a square VCSELs with the cavity size of 30 × 30 μm^2 and the corresponding path-length distributions at the operating temperature of 290 K, 275 K, and 260 K.

are mainly affected by both injection currents and operating temperature. As proposed in [12], the level of the injection current is to determine the coupling effects between the optical modes and the spontaneous emission. The emission spectra presented deeper scale of the modulation depth at higher injection current. The path-length distributions then exhibit more and more resonant peaks corresponding to photon POs as the injection current increases. At subthreshold current, the largest number of the discernible photon POs can be displayed in the path-length distribution. On the other hand, the main effect of changing the operating temperature is to determine the frequency detuning $\Delta\omega = \omega - \omega_c$, where ω is the central frequency of the gain profile and ω_c is the frequency of the fundamental cavity mode. To see the influence of the operating temperature, we measured the subthreshold emission spectra for a square VCSELs with the cavity size of 30 × 30 μm^2 and calculated the corresponding path-length distributions at the operating temperature of 290 K, 275 K, and 260 K, as shown in Fig. 1. It was found that when the operating temperature was decreased, the profile of the emission spectrum apparently shifted to the regime with large transverse wave number and the width of the spectrum became much narrower. This makes the resonant peaks with small transverse wave number to have insignificant intensity. As a result, the path-length distribution can present only a few number of discernible photon POs at low operating temperature. To sum up, the effects of injection currents and operating temperature are to change the coupling condition between the optical transverse modes and the spontaneous emission, but not to

#251204 Received 30 Sep 2015; revised 9 Dec 2015; accepted 9 Dec 2015; published 4 Jan 2016

affect the effective strength of the confinement which is the intrinsic character of the device. Accordingly, in this investigation, we operated the VCSELs just below the lasing threshold at the temperature about 290 K such that the measured subthreshold emission spectra can present sharp resonant peaks extended over a wide range of transverse wave numbers. For most devices, the levels of the subthreshold current should be greater than 95% of the threshold current but would have exceptions. The impact of the level of the subthreshold current is worthy to deeply investigate and must be left for future work.

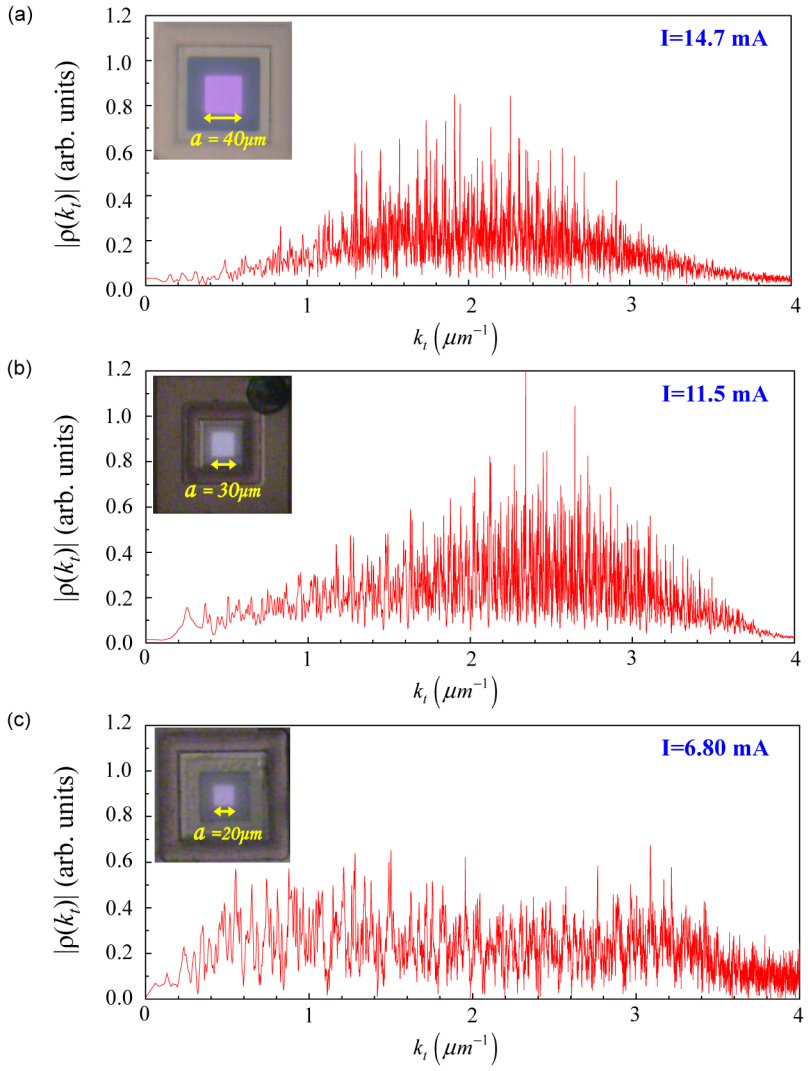

Fig. 2. The optical microscope photographs and the experimental subthreshold emission spectra $\rho(k_t)$ for the VCSELs with aperture size of (a) 40 × 40 μm^2, (b) 30 × 30 μm^2, and (c) 20 × 20 μm^2.

Figure 2 depicts the optical microscope photographs and the experimental subthreshold emission spectra $\rho(k_t)$ for the VCSELs with the cavity size of 40 × 40 μm^2[Fig. 2(a)], 30 × 30 μm^2[Fig. 2(b)] and 20 × 20 μm^2 [Fig. 2(c)]. The threshold current for these VCSELs are about 15.20 mA [$a = 40$ μm], 11.80 mA [$a = 30$ μm], and 7.30 mA [$a = 20$ μm], respectively. The current levels of the measured subthreshold emission spectra were been

#251204 Received 30 Sep 2015; revised 9 Dec 2015; accepted 9 Dec 2015; published 4 Jan 2016

displayed in Fig. 2. Since the average mode spacing is inversely proportional to the effective area of the confinement, the overall mode number in the subthreshold emission spectrum can be seen to be less for a smaller-aperture VCSEL.

By using the experimental spectra $\rho(k_t)$, the path-length spectra $|\rho_{FT}(\mathrm{L})|$ were numerically calculated with the Fourier transform. Figure 3 illustrates the path-length spectra

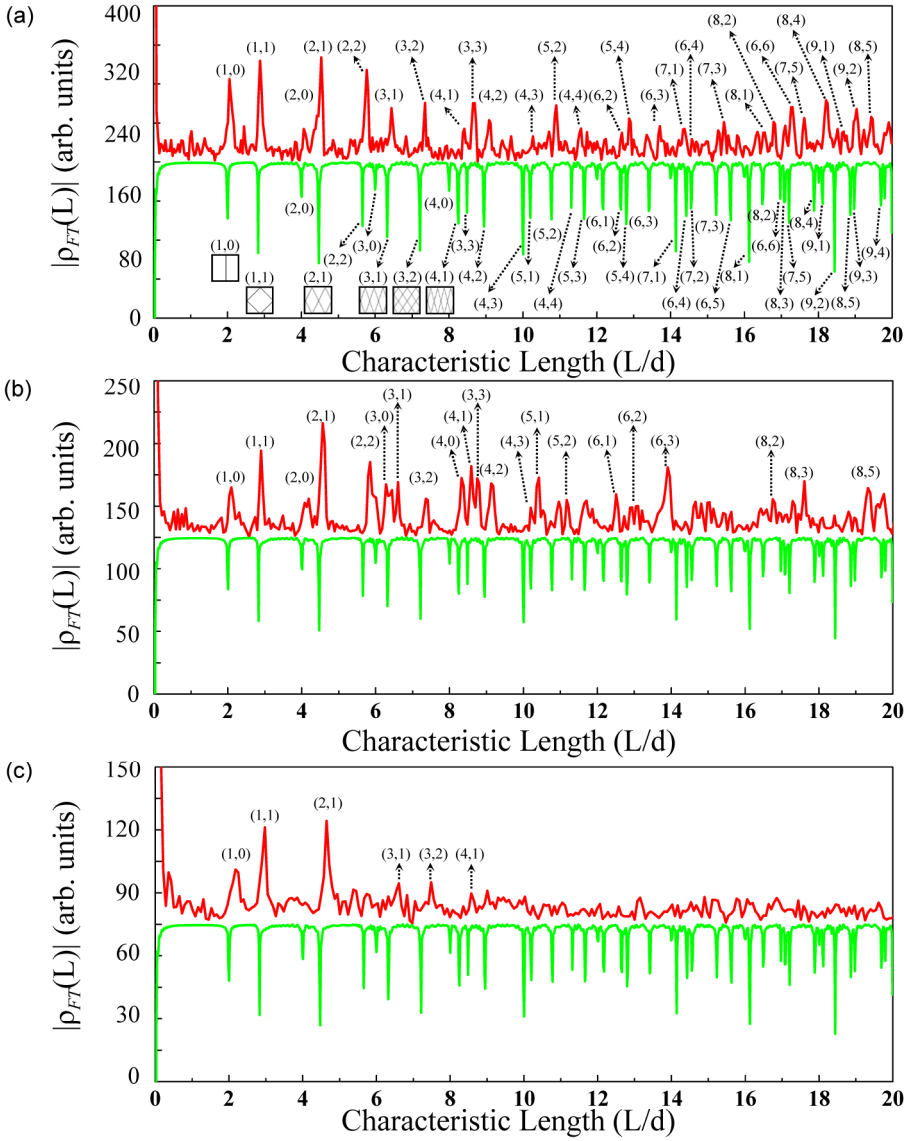

Fig. 3. The path-length spectra of the experimental spectra for the square-shaped VCSELs with aperture size of (a) 40 × 40 μm^2, (b) 30 × 30 μm^2, and (c) 20 × 20 μm^2. The mirror image in each figure displays the path-length distribution of an infinite potential quantum billiard.

$|\rho_{FT}(\mathrm{L})|$ for the VCSELs with the cavity size of 40 × 40 μm^2[Fig. 3(a)], 30 × 30 μm^2 [Fig. 3(b)], and 20 × 20 μm^2[Fig. 3(c)]. As discussed in previous reports [12, 13, 17–19], the peak positions in the path-length spectrum correspond to the geometric lengths of classical POs. For square quantum billiards [19], the geometric lengths of classical POs are given by

#251204 Received 30 Sep 2015; revised 9 Dec 2015; accepted 9 Dec 2015; published 4 Jan 2016

$L(p,q) = 2d\sqrt{p^2+q^2}$, where p and q are two positive integers describing the number of collisions on the two orthogonal walls and d is the length of the square boundary. To make a comparison with the infinite potential quantum-billiard spectrum, we calculated the path-length distribution for a square quantum billiard, as plotted in the mirror images of Fig. 3. The peak positions in the experimental spectrum $\left|\rho_{FT}(\mathrm{L})\right|$ can be seen to slightly deviate from the actually geometric lengths $L(p,q)$. To quantitatively describe this deviation, we recorded some geometric lengths $L(p,q)$ from the path-length distributions for the experimental results and the theoretical analysis, as listed in Table 1. The deviation is found to be more prominent for the VCSELs with smaller cavity size than larger cavity size. More importantly, it is clear that the overall number of the resonant peaks in the spectrum $\left|\rho_{FT}(\mathrm{L})\right|$ decreases with decreasing the cavity size. This result indicates that the effective confinement strength can be straightforwardly revealed in the experimental path-length spectrum. It should be mentioned that even though this observation is quite similar to the change of the path-length distribution with injection current in [12], the two cases have different physical origins. The result of this work arises from the varying of the effective confinement strength, whereas the latter case results from the different coupling strengths between the optical modes and the spontaneous emission. In the following, we perform theoretical analyses for quantum billiards with equivalent confinement strengths to make a detailed comparison with experimental observations.

Table 1. Some geometric lengths *L*(*p*,*q*)[a]

	L(1,0)	*L*(1,1)	*L*(2,1)	*L*(3,1)	*L*(3,2)	*L*(4,1)
Infinite potential quantum billiard	2.00d	2.83d	4.48d	6.32d	7.21d	8.25d
VCSEL with $a = 40$ μm	2.04d	2.88d	4.53d	6.42d	7.35d	8.37d
VCSEL with $a = 30$ μm	2.09d	2.91d	4.57d	6.54d	7.42d	8.42d
VCSEL with $a = 20$ μm	2.16d	2.98d	4.65d	6.61d	7.53d	8.61d

[a]From Fig. 2(a)-2(c)

3. Theoretical analyses

Since the finite-potential square quantum billiards cannot be analytically solved, the method proposed by Marcatili [26] was used here to calculate the eigenvalues. The Schrödinger equation for finite-potential quantum billiards is given by

$$\left[-\frac{\hbar^2}{2\mu}\nabla^2 + \left(E - V(\vec{\mathbf{r}})\right)\right]\psi(\vec{\mathbf{r}}) = 0, \tag{1}$$

where μ is the mass of the particle and the 2D potential well given by

$$V(\vec{\mathbf{r}}) = \begin{cases} 0 & \text{if } \vec{\mathbf{r}} \in \mathbf{I} \\ V_B & \text{if } \vec{\mathbf{r}} \notin \mathbf{I} \end{cases}. \tag{2}$$

For a square shape billiard, the domain **I** is set to be enclosed by the vertices at $(\pm a/2, \pm a/2)$ and $(\pm a/2, \mp a/2)$, where a is the side length. The eigenfunctions are approximately

#251204 Received 30 Sep 2015; revised 9 Dec 2015; accepted 9 Dec 2015; published 4 Jan 2016

expressed as the product of x- and y-dependent functions, i.e., $\psi_{m,n}(\vec{\mathbf{r}}) = X_m(x)Y_n(y)$. The boundary condition requests that the wave functions $X_m(x)$ and $Y_n(y)$ are continuous at the boundaries of well interfaces $x = \pm a/2$ and $y = \pm a/2$. Another boundary condition is that the derivatives of the wave functions, $dX_m(x)/dx$ and $dY_n(y)/dy$, should also be continuous at the boundaries. As a result, the eigenvalue equations for determining the quantized wavenumbers $k_{x,m}$ and $k_{y,n}$ in the x- and y-directions are given by

$$\begin{aligned} k_{x,m}\frac{a}{2} &= \frac{m\pi}{2} + \tan^{-1}\left(\frac{\alpha_{x,m}}{k_{x,m}}\right), \\ k_{y,n}\frac{a}{2} &= \frac{n\pi}{2} + \tan^{-1}\left(\frac{\alpha_{y,n}}{k_{y,n}}\right) \end{aligned} \tag{3}$$

where $\alpha_{x,m} = \sqrt{V_B - k_{x,m}^2\hbar^2/2\mu}$ and $\alpha_{y,n} = \sqrt{V_B - k_{y,n}^2\hbar^2/2\mu}$. In the limit of $V_B \to \infty$, the quantized wavenumbers $k_{x,m}$ and $k_{y,n}$ can be easily found to be $m\pi/a$ and $n\pi/a$, respectively, as the consequence of infinite-potential square quantum billiards. The number of allowed eigenmodes is directly related to the confinement strength of a billiard. From Eq. (3), the restrictions of $\alpha_{x,m} \geq 0$ and $\alpha_{y,n} \geq 0$ limit the allowed wavenumbers to be given by $k_{x,m} \leq \sqrt{2\mu V_B}/\hbar$ and $k_{y,n} \leq \sqrt{2\mu V_B}/\hbar$. Using the approximation of $k_{x,m} = m\pi/a$ and $k_{y,n} = n\pi/a$, the maximum allowed mode indices M and N in the x-direction and y-directions can be obtained as $M = N = a\sqrt{2\mu V_B}/\pi\hbar$. As a consequence, the total number of the allowed eigenmodes can be estimated as $M \times N = 2\mu V_B A/(\pi\hbar)^2$, where A is the area of the billiard. In other words, the total number of the confined eigenmodes is proportional to the product of the area A and the potential height V_B. In a precise way, the total number of the confined eigenmodes can be numerically calculated. Figure 4 shows the calculated results for the number of the allowed eigenmodes as a function of side length a for a given $V_B = 0.1$eV and as function of potential height V_B for a given $a = 150\,a_0$, where $a_0 = 4\pi\varepsilon_0\hbar^2/e^2m_e$ is the Bohr radius. Calculated results reveal that the number of the allowed modes is approximately proportional to the square of the size a for a given V_B and is nearly proportional to the potential barrier V_B for a given a. Note that the phenomenon of the staircase in Fig. 3 clearly comes from the level spacing induced by the confinement.

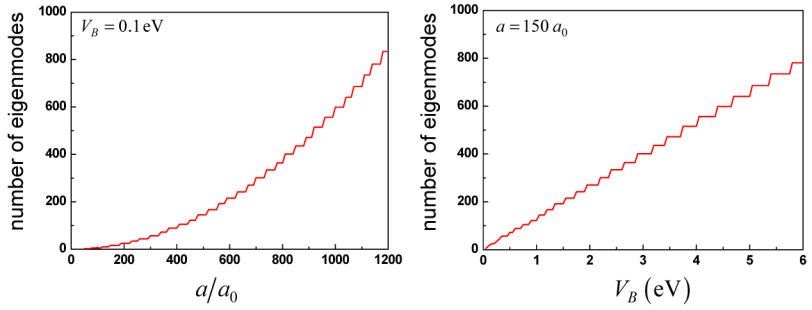

Fig. 4. The number of allowed eigenmodes with respect to the size a and the potential barrier V_B. Note that the size is normalized by the Bohr radius with $a_0 = 4\pi\varepsilon_0\hbar^2/e^2m_e$

#251204 Received 30 Sep 2015; revised 9 Dec 2015; accepted 9 Dec 2015; published 4 Jan 2016

By using the calculated eigenvalues $k_{m,n} = \sqrt{\left(k_{x,m}\right)^2 + \left(k_{y,n}\right)^2}$, the path-length distribution can be evaluated with the expression of $\rho_{FT}(L) = \sum_{m,n} e^{ik_{m,n}L}$. To make a systematic comparison with experimental results shown in Fig. 2, the equivalent side length *a* needed to be found for a given V_B. The equivalent size length *a* can be obtained from the analogy that the numbers of the allowed for 1D quantum box and 1D dielectric waveguide are given by $N = a\sqrt{2\mu V_B}/\pi\hbar$ and $N = dk\sqrt{\left(n_1^2 - n_2^2\right)}/\pi$, respectively. Consequently, for a given V_B = 0.1eV the equivalent size lengths of square quantum billiards are found to be $1620\,a_0$, $1080\,a_0$, and $540\,a_0$ to correspond to the VCSELs with the aperture size of 40 × 40 μm^2, 30 × 30 μm^2, and 20 × 20 μm^2, respectively. Figure 5 shows the calculated path-length spectra for square quantum billiards with V_B = 0.1eV and the size lengths of $1620\,a_0$, $1080\,a_0$, and $540\,a_0$. Experimental results shown in Fig. 3 are depicted in the Fig. 5 with mirror images for comparison. It can be seen that the theoretical path-length distributions for finite-potential quantum billiards positions are in good agreement with experimental observations for all cases over a wide range. The good agreement validates that the broad-area VCSELs can be employed as an experimental manifestation of quantum billiards with finite confinement strength. Meaningfully, it is worthy to mention that this work clearly demonstrates the role of finite confinement strength in VCSELs and quantum billiards, which can provide a deep insight into laser physics and quantum chaos in real world.

#251204 Received 30 Sep 2015; revised 9 Dec 2015; accepted 9 Dec 2015; published 4 Jan 2016

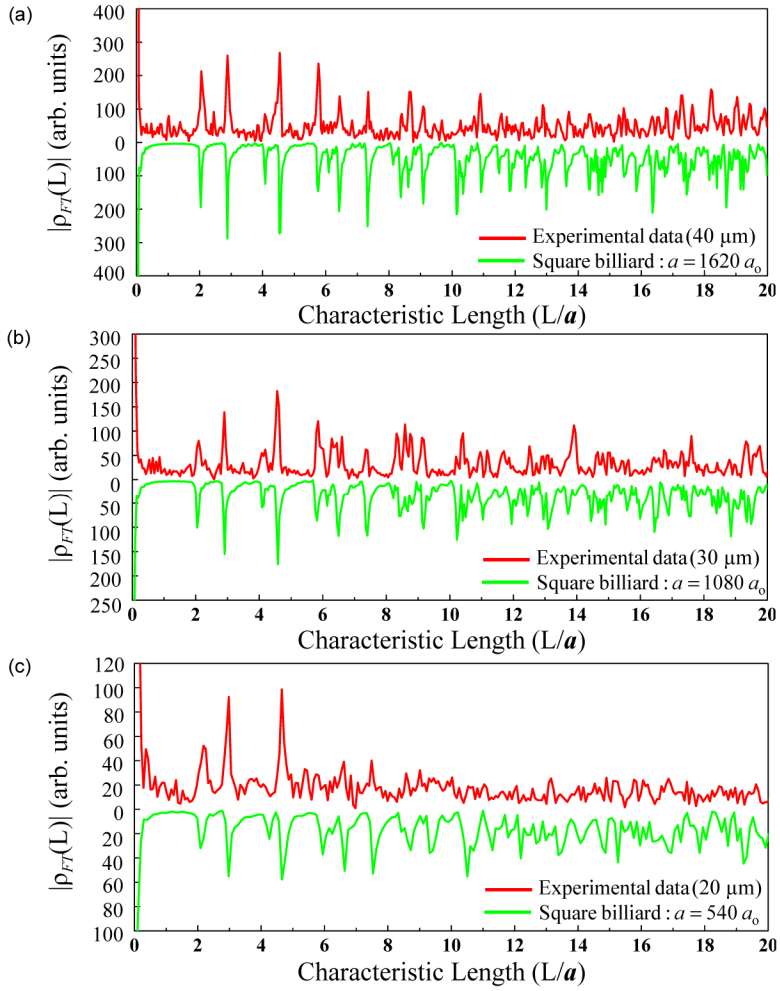

Fig. 5. Calculated path-length spectra for square quantum billiards with V_B = 0.1eV and the size lengths of (a) $1620\,a_0$, (b) $1080\,a_0$, and (c) $540\,a_0$. Experimental results are depicted with mirror images for comparison.

4. Conclusion

In conclusion, we have designed broad-area square-shaped VCSELs with different cavity sizes to explore the subthreshold emission spectra and the Fourier transformed path-length spectra. The confinement strengths controlled by the cavity size have been found to significantly affect the number of the resonant peaks in the path-length spectra. The experimental results have been confirmed to agree well with the theoretical predictions of square quantum billiards with equivalent confinement strengths. The good agreement between the experimental results and theoretical calculations reveals that the broad-area VCSELs can be utilized to analogously explore the influence of the finite confinement on the mesoscopic phenomena of finite-potential quantum billiards.

Acknowledgments

The authors thank the Ministry of Science and Technology, Taiwan, R.O.C. for their financial support of this research under Contract No. MOST103-2112-M-009-016-MY3.

#251204 Received 30 Sep 2015; revised 9 Dec 2015; accepted 9 Dec 2015; published 4 Jan 2016